

Constraining Primordial Magnetism

J. Richard Shaw^{1,2,*} and Antony Lewis^{3,†}

¹*Kavli Institute for Cosmology, Madingley Road, Cambridge, CB3 0HA, UK.*

²*Institute of Astronomy, Madingley Road, Cambridge, CB3 0HA, UK.*

³*Astronomy Centre, University of Sussex, Brighton, BN1 9QH, UK*

(Dated: June 23, 2010)

Primordial magnetic fields could provide an explanation for the galactic magnetic fields observed today, in which case they may also leave interesting signals in the CMB and the small-scale matter power spectrum. We discuss how to approximately calculate the important non-linear magnetic effects within the guise of linear perturbation theory, and calculate the matter and CMB power spectra including the SZ contribution. We then use various cosmological datasets to constrain the form of the magnetic field power spectrum. Using solely large-scale CMB data (WMAP7, QUaD and ACBAR) we find a 95% CL on the variance of the magnetic field at 1 Mpc of $B_\lambda < 6.4$ nG. When we include SPT data to constrain the SZ effect, we find a revised limit of $B_\lambda < 4.1$ nG. The addition of SDSS Lyman- α data lowers this limit even further, roughly constraining the magnetic field to $B_\lambda < 1.3$ nG.

I. INTRODUCTION

Magnetic fields are observed at the 10^{-6} G level in galaxies and clusters, not just in the local Universe, but up to a redshift of $z \sim 0.7-2$ [1]. Production of magnetic fields within a formed galaxy is extremely difficult, and the consensus is that they are amplified from pre-galactic seed fields [2]. One interesting possibility is that these seed fields were primordial in origin, formed in the very early Universe.

The observations of magnetic fields up to a redshift of $z \sim 2$ are particularly interesting as the fields have amplitudes ($B \sim 10\mu\text{G}$) comparable to those observed locally [3]. This evidence seems to disfavour a large dynamo amplification, requiring a larger seed field to produce today's magnetic fields. In the extreme case of there being no dynamo amplification, adiabatic contraction alone could amplify a pre-galactic field of around 1 nG (comoving) to the required level.

A stochastic primordial magnetic field would source scalar, vector and tensor modes, giving rise to both temperature and polarisation perturbations in the Cosmic Microwave Background [4–8], and perturbing the matter distribution in the local universe [9]. Our aim in this paper is to see what limits current data places on the level of magnetic fields in the early universe, and whether this is compatible with a scenario where galactic magnetic fields are seeded by primordial magnetic fields. Similar work has been carried out in the past [10–12], finding field strengths of several nG to be consistent with current CMB data.

This work will depend heavily on the results of a previous paper [8], and will use the same conventions and notation. Where it is necessary to use perturbation theory we use a gauge invariant notation [13, 14] similar to

the Conformal Newtonian Gauge. In this work we limit ourselves to a flat Λ CDM universe.

II. NON-LINEAR FIELD EVOLUTION

We will consider a stochastic magnetic field $B^i(x^j, \tau)$ generated by some mechanism in the very early Universe. As for all the periods of interest the Universe contains a highly ionised plasma, we can use the MHD equations to describe the behaviour of the magnetic field. At linear order in the magnetic field

$$\frac{\partial}{\partial \tau} [a^2 B^i(\mathbf{x}, \tau)] = 0, \quad (1)$$

and this motivates the definition of a comoving magnetic field, $\hat{B}^i(\mathbf{x}, \tau) = a^2 B^i(\mathbf{x}, \tau)$ which is time independent at linear order. Using this we can write the non-zero components of the magnetic energy-momentum tensor as

$$T_0^0 = -\frac{1}{8\pi a^4} \hat{B}^2(\mathbf{x}), \quad (2a)$$

$$T_j^i = \frac{1}{4\pi a^4} \left(\frac{1}{2} \hat{B}^2(\mathbf{x}) \delta_j^i - \hat{B}^i(\mathbf{x}) \hat{B}_j(\mathbf{x}) \right). \quad (2b)$$

As there is no magnetic field on the background, the perturbations of the stochastic background are manifestly gauge invariant. We construct density and anisotropic stress perturbations, Δ_B and Π_B , defined by

$$T_0^0 = -\rho_\gamma \Delta_B, \quad (3a)$$

$$T_j^i = p_\gamma (\Delta_B \delta_j^i + \Pi_B^i{}_j), \quad (3b)$$

where we include the factors of ρ_γ and p_γ to take account of the a^{-4} factors. As usual the anisotropic stress $\Pi_B^i{}_j$ can be decomposed into scalar, vector and tensor contributions.

At higher order the comoving magnetic field obeys

$$\begin{aligned} \partial_\tau \hat{B}^i &= [\nabla \times (\mathbf{v} \times \hat{\mathbf{B}}) + \eta \nabla^2 \hat{\mathbf{B}}]^i \\ &= \epsilon^{ijk} \epsilon_{klm} \partial_j (v^l \hat{B}^m) + \eta \partial_j \partial^j \hat{B}^i \end{aligned} \quad (4)$$

*Electronic address: jrs65@ast.cam.ac.uk

†URL: <http://cosmologist.info>

where \mathbf{v} is the baryon velocity and η is the magnetic diffusivity. In a highly conductive medium η is negligible and so we will set it to zero from here onwards. As (4) is non-linear the magnetic field evolution cannot be treated accurately in the standard linearised Einstein-Boltzmann approach. The standard approach is to separate the higher order evolution of the magnetic field into two effects that are physically well-motivated, a damping due to the radiation viscosity, and the effect of the magnetic Jeans length. For extended discussions, see [15–17], and especially [18] to which we follow a similar line of reasoning below.

First let us construct Δ^{ij} , a quadratic combination of the magnetic field

$$\Delta^{ij} = \frac{1}{4\pi\rho_\gamma a^4} \hat{B}^i \hat{B}^j, \quad (5)$$

with the normalisation chosen such that it is conveniently close to the magnetic perturbations

$$\begin{aligned} \Delta_B &= \frac{1}{2} \Delta_k^k, \\ \Pi_B^{ij} &= \Delta_k^k \delta^{ij} - 3\Delta^{ij}. \end{aligned} \quad (6)$$

We are interested in the time evolution of Δ^{ij} , and thus want to calculate the derivative $\dot{\Delta}^{ij} = \frac{1}{2\pi\rho_\gamma a^4} \hat{B}^{(i} \partial_\tau \hat{B}^{j)}$, where the parentheses indicate symmetrisation with respect to the enclosed indices. It will be useful to repress (4) by expanding the Levi-Civita symbols

$$\partial_\tau \hat{B}^i = \hat{B}^k (\partial_k v^i) - v^k (\partial_k \hat{B}^i) - \hat{B}^i \partial_k v^k. \quad (7)$$

Using (7) we can calculate the time derivative of Δ^{ij}

$$\dot{\Delta}^{ij} = 2(\partial_k v^{(i} \Delta^{j)k}) - 2(\partial_k v^k \Delta^{ij} - v^k (\partial_k \Delta^{ij})). \quad (8)$$

Using the definitions of (6) we can split the above into equations for each of the perturbations Δ_B and Π_B . Firstly

$$\dot{\Delta}_B = -\frac{4}{3} \Delta_B \theta_b - v^k (\partial_k \Delta_B) - \frac{1}{3} \sigma_{kl} \Pi_B^{kl} \quad (9)$$

where we have only included terms up to second order, and we have decomposed

$$\partial_i v_j = \frac{1}{3} \theta_b \delta_{ij} + \sigma_{ij} + \omega_{ij} \quad (10)$$

at linear order. Physically θ_b is the divergence of the baryon 3-velocity, and σ_{ij} is its shear; we will neglect the antisymmetric vorticity tensor ω_{ij} . The magnetic anisotropic stress evolves as

$$\begin{aligned} \dot{\Pi}_B^{ij} &= -\frac{4}{3} \theta_b \Pi_B^{ij} - v^k \partial_k \Pi_B^{ij} - 4\sigma^{ij} \Delta_B \\ &\quad + 2\sigma_k^{(i} \Pi_B^{j)k} - \frac{2}{3} \sigma_{kl} \Pi_B^{kl} \delta^{ij}. \end{aligned} \quad (11)$$

The first effect to consider is that as perturbations collapse the magnetic field lines will also be compressed,

leading to greater pressure opposing to gravitational collapse, which leads to a magnetic Jeans length. We can see that the relevant terms in (9) and (11) are the first terms on the right-hand side of each, to this end we will largely neglect the other terms. This leaves

$$\begin{aligned} \dot{\Delta}_B &= -\frac{4}{3} \Delta_B \theta_b, \\ \dot{\Pi}_B^{ij} &= -\frac{4}{3} \Pi_B^{ij} \theta_b. \end{aligned} \quad (12)$$

We can use the baryon density evolution equation

$$\dot{\Delta}_b = -\theta_b + 3\dot{\Phi} \quad (13)$$

to replace θ_b , and neglect $\dot{\Phi}$ on the small scales of interest, finding solutions for the magnetic perturbations

$$\begin{aligned} \Delta_B &= \Delta_{B,0} \exp\left(\frac{4}{3} \Delta_b\right) \\ \Pi_B^{ij} &= \Pi_{B,0}^{ij} \exp\left(\frac{4}{3} \Delta_b\right), \end{aligned} \quad (14)$$

where $\Delta_{B,0}$ and $\Pi_{B,0}$ are the magnetic perturbations at some initial time where the baryon perturbation Δ_b was much smaller than its present value. The linearised equation for the evolution of the baryon velocities in Fourier space is

$$\begin{aligned} \dot{\theta}_b &= -\mathcal{H} \theta_b + k^2 c_{s,b}^2 \Delta_b + k^2 \Psi + R\tau_c^{-1} (\theta_\gamma - \theta_b) \\ &\quad + \frac{1}{2} k^2 R \left(\frac{1}{2} \Delta_B - \frac{1}{3} \Pi_B^{(0)} \right) \end{aligned} \quad (15)$$

where τ_c is defined as $\tau_c = 1/(an_e \sigma_T)$, $c_{s,b}$ the baryon sound speed, $R = 4\rho_\gamma/3\rho_b$, and the last term is the magnetic interaction, the Lorentz force. To include the magnetic evolution in this, we need to somehow linearise (14), which we do by expanding up to second order, and replace the magnetic perturbation with its expectation (smoothed at the relevant scale) in the higher order terms only. In Fourier space this leaves

$$\Delta_B = \Delta_{B,0} + \frac{4}{3} \langle \Delta_{B,0} \rangle_k \Delta_b, \quad (16)$$

$$\Pi_B^{ij} = \Pi_{B,0}^{ij}. \quad (17)$$

The equation for Π_B has only the lowest order term as $\langle \Pi_{B,0} \rangle_k = 0$. There is some justification for this— as Δ_B is always positive, whereas Δ_b has zero mean, we expect there to be a significant coherent term from the large-scale magnetic energy density times the baryon perturbation at the scale of interest.

Inserting (16) into (15) gives

$$\begin{aligned} \dot{\theta}_b &= -\mathcal{H} \theta_b + k^2 c_{s,b}^2 \Delta_b + k^2 \Psi + R\tau_c^{-1} (\theta_\gamma - \theta_b) \\ &\quad + \frac{1}{2} k^2 R \left(\frac{1}{2} \Delta_{B,0} - \frac{1}{3} \Pi_{B,0}^{(0)} \right) + \frac{2}{9} k^2 v_A^2 \Delta_b \end{aligned} \quad (18)$$

where we have defined the Alfvén velocity v_A as

$$v_A^2 = \frac{1}{4\pi\rho a^4} \langle \hat{B}^2 \rangle_k = \frac{3}{2} R \langle \Delta_{B,0} \rangle_k, \quad (19)$$

where ρ is the density of the conducting fluid. The last equality comes from the fact that during matter domination $\rho = \rho_b$. The overall effect of including the magnetic Jeans effect is to appear as the standard evolution equation (15) with a new effective sound speed $c_s^2 \rightarrow c_s^2 + \frac{2}{9} v_A^2$. This agrees with other approximate treatments in the literature up to the factor of $\frac{2}{9}$ [15, 17]. As this effect is non-linear, even when evolving the standard adiabatic mode we must add continue to add in the Alfvén velocity term.

Radiation free streaming is particularly important for magnetic fields, and is the most important source of damping on large scales [16]. Prior to free-streaming, there are many photon-baryon scatterings per wavelength, and the radiation and baryons appear like a single tightly-coupled conducting fluid. However, when the photons start to free stream they decouple from the baryon fluid and this becomes the sole conducting fluid. Whilst the baryons are no longer tightly coupled to the photons, there is still enough scattering to exert a significant drag force on the fluid, and this causes damping on propagating magnetic waves.

When the photons decouple from a particular scale, the fluid no longer feels the radiation pressure, and the magnetic pressure dominates the baryon pressure for $B \gtrsim 0.1$ nG. In this regime, in addition to Alfvén modes, magneto-acoustic modes are also significant.

Properly accounting for the damping in the radiation free-streaming regime requires the use of the full Boltzmann system for the photons, a procedure that is complicated by the necessity of including non-linear magnetic effects. Instead we use the prescription of [15], who analyse the evolution of Alfvén modes in the presence of a homogeneous radiation drag force. They find that the magnetic field on small scales damped approximately as

$$\hat{B}^i(\mathbf{k}) = \hat{B}_0^i(\mathbf{k}) \exp \left(-k^2 \int^{\tau_*} v_A^2 \tau_c d\tau \right), \quad (20)$$

where v_A and τ_c are defined above, and τ_* is the time of last scattering. For magneto-acoustic modes, the damping is similar to that of (20) with the Alfvén velocity v_A replaced with the baryon sound speed $c_{s,b}$, causing them to damp on smaller scales [15, 16]. For simplicity, we will treat the field as damping solely on the largest scale, that of the Alfvén modes.

To account for this damping in our work, we allow the linear perturbations Δ_B and Π_B to evolve. This is in contrast to other work in the literature [5, 6, 10] where the perturbations are constant for all time and the damping is imposed as a cut off on the initial power spectrum. This is implemented by constructing effective differential

equations for the two perturbations for $\tau < \tau_*$ ¹

$$\begin{aligned} \dot{\Delta}_B &= -2k^2 v_A^2 \tau_c \Delta_B, \\ \dot{\Pi}_B &= -2k^2 v_A^2 \tau_c \Pi_B. \end{aligned} \quad (21)$$

For $\tau > \tau_*$, we set $\dot{\Delta}_B$ and $\dot{\Pi}_B$ to zero, as after recombination there is less than one scattering per Hubble time and the damping is negligible. To ensure that energy conservation is maintained we presume that this is transferred equally into the photon-baryon fluid. We modify the baryon density equation to

$$\dot{\Delta}_b = -\theta_b + 3\dot{\Phi} + \frac{2k^2}{1+R^{-1}} v_A^2 \tau_c \Delta_B, \quad (22)$$

and the photon density equation to

$$\dot{\Delta}_\gamma = -\frac{4}{3} \theta_\gamma + 4\dot{\Phi} + \frac{2k^2}{1+R^{-1}} v_A^2 \tau_c \Delta_B, \quad (23)$$

where we have added the final term in both of the above equations. Practically, ensuring energy conservation makes little difference to the results.

III. MAGNETIC MATTER POWER SPECTRUM

Using the above modifications to the evolution equations we are able to calculate matter power spectra including approximate treatments of the important non-linear effects. The remaining input is the statistics of the initial magnetic perturbations Δ_B and Π_B . We assume that at some early time the comoving magnetic field power spectrum is described by a power spectrum

$$\langle \hat{B}_i(\mathbf{k}) \hat{B}_j^*(\mathbf{k}') \rangle = (2\pi)^3 \delta(\mathbf{k} - \mathbf{k}') \frac{P_{ij}(\hat{k})}{2} P_B(k), \quad (24)$$

where $P_{ij} = \delta_{ij} - \hat{k}_i \hat{k}_j$, and we will not consider helicity. The magnetic field power spectrum is

$$P_B(k) = A k^{n_B}. \quad (25)$$

We will use the spectral index n_B as defined, but it is conventional to give the amplitude of the spectrum in terms of the variance B_λ^2 of the magnetic field strength at a scale λ (we choose $\lambda = 1$ Mpc to agree with the bulk of the literature). This gives

$$A = \frac{(2\pi)^{n_B+5} B_\lambda^2}{2\Gamma\left(\frac{n_B+3}{2}\right) k_\lambda^{n_B+3}}. \quad (26)$$

¹ Though we base our treatment on that of [15], it is worth noting that approximately the same result for Δ_B can be derived from (12) and (15), using the same approximation as in (16) and those within [15] (notably, homogeneous baryons $\Delta_b \sim 0$ and drag $\theta_\gamma \sim 0$, and terminal velocity $\dot{\Delta}_B \sim 0$) in the overdamped regime.

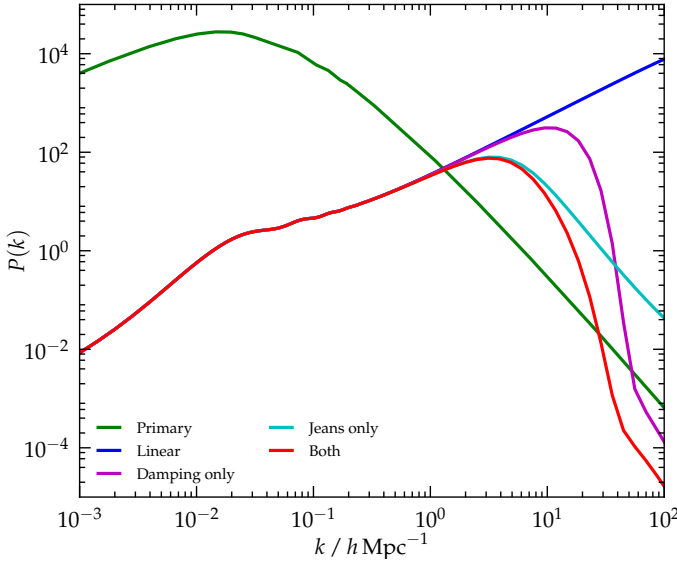


FIG. 1: The additional non-linear effects modify the magnetic power spectrum. We plot: the linear only behaviour; the diffusion damping of the magnetic field; the magnetic pressure support; and both effects combined. For comparison we also include the primary adiabatic mode.

To calculate the two required power spectra $P_{\Delta_B}(k)$, $P_{\Pi_B}(k)$ and the cross spectrum $P_{\Delta_B\Pi_B}(k)$ requires convolutions of the magnetic power spectrum. We use the results of a previous paper [8], which allows us to reduce the convolution into a dimensionless integral depending only on n_B . We numerically evaluate these at a large number of values such that we can accurately interpolate to find power spectra at an arbitrary n_B . It is important to note that as we are including the damping and Jeans' effects in the evolution of the magnetic perturbations we can safely avoid imposing a cutoff in the initial power spectrum as used in other work [5, 12].

In Fig. 1 we show the consequence of the two non-linear effects on the matter power spectrum. The first thing to note is that the linear theory magnetic power spectrum grows as $P(k) \propto k$. On sub-horizon scales during matter domination, we can combine the evolution equations for baryons and dark matter to give an equation for the total matter perturbation $\Delta_m = R_b\Delta_b + R_c\Delta_c$

$$\ddot{\Delta}_m + \mathcal{H}\dot{\Delta}_m - \frac{3}{2}\mathcal{H}^2\Delta_m = \frac{\rho_\gamma}{\rho_m}k^2L_B, \quad (27)$$

where the Lorentz force $L_B = \frac{2}{3}(\frac{1}{3}\Pi_B - \Delta_B)$, and we have also neglected pressure terms in $c_{s,b}^2$. In these limits the equation has a simple solution for the magnetic mode

$$\Delta_m = R_bL_B \frac{\rho_\gamma(\tau_i)}{\rho_b(\tau_i)} (k\tau_i)^2 \left[\frac{1}{10} \left(\frac{\tau}{\tau_i} \right)^2 + \dots \right] \quad (28)$$

where we have included only the leading order term, and τ_i is the time when the mode starts to grow significantly. This is the time that the baryon perturbation decouples

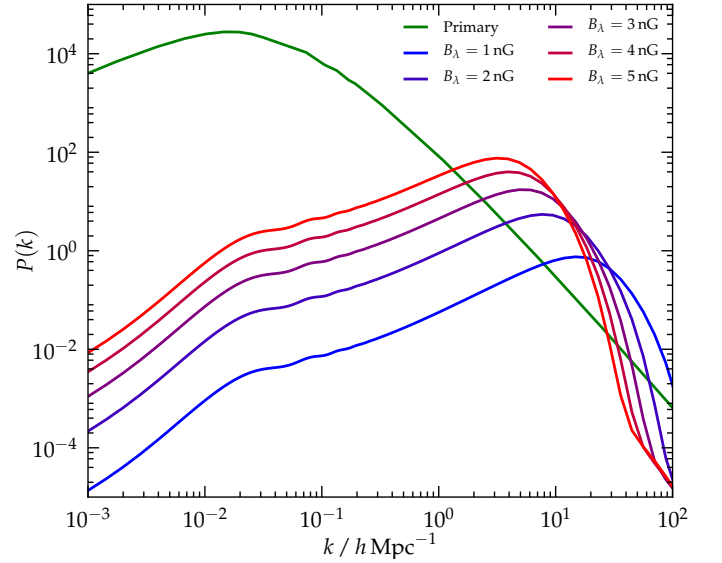


FIG. 2: The full matter power spectrum with all non-linear effects at a variety of magnetic field strengths between $B_\lambda = 1$ – 5 nG. We have held the magnetic spectral index constant at $n_B = -2.9$. The power spectrum amplitude increases strongly with that of the magnetic field, however the two scales associated with the diffusion damping and magnetic Jeans length also increase rapidly.

from the photons. Provided this time is similar across a range of scales (correct for larger scales), we can expect $P_m(k) \propto k^4 P_{L_B}(k)$; for nearly scale invariant magnetic field spectra this gives $P_m(k) \propto k$.

The effect of including the magnetic pressure increases the Jeans length, and thus causes smaller scales to oscillate. In matter domination, the comoving magnetic Jeans wavenumber is constant and thus larger k grow very little after recombination. On even larger scales the diffusion damping of the magnetic fields causes the source for the later growth of the magnetic fields to be exponentially suppressed. This leads to much slower growth in the matter perturbations, and an effective cutoff beyond which there are no significant perturbations sourced. The scales at which these effects start roughly agree with the estimates of [15, 17, 19], where both are expected to scale like $k_c \propto B_\lambda^{-(n+5)/2}$.

In Fig. 2 and Fig. 3, we plot the effect on the matter power spectrum of the amplitude and tilt of the magnetic spectrum. Fig. 2 shows that the relative contrast between the peak magnetic and primary contributions stay roughly constant as the amplitude B_λ is varied. This occurs as a consequence of the fact that the matter power spectrum at the damping cutoff is $\propto B_\lambda^4 k_c$, whilst the primary spectrum $\propto k_c^{-3}$. However as the damping wavenumber $k_c \propto B_\lambda^{-1}$ for nearly scale invariant spectra, the ratio between the two is constant.

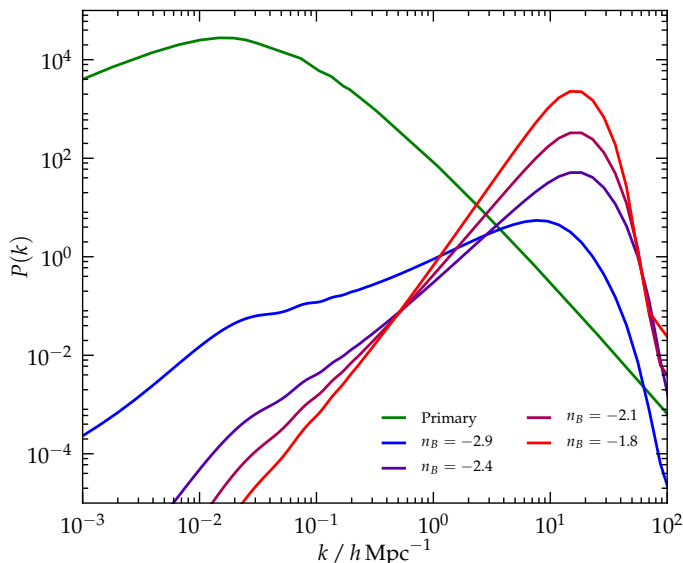


FIG. 3: The full matter power spectrum with all non-linear effects at a variety of magnetic spectral indices between $n_B = -2.9$ to -1.8 . The amplitude is fixed at $B_\lambda = 1$ nG.

IV. RESULTS

We have used versions of CAMB [20] and CosMoMC [21] modified to generate the magnetic contributions to both the CMB angular power spectrum and the matter power spectrum². We sample with a flat prior in the standard set of cosmological parameters $\{\Omega_b h^2, \Omega_c h^2, \theta, \tau, n_s, \log(10^{10} A_s)\}$, assuming a flat Λ CDM universe. To describe the magnetic fields we supplement this with three parameters, the magnetic power spectrum amplitude B_λ and spectral index n_B . We also need to specify the production time of the magnetic fields τ_B to calculate the passive modes. For this we use a proxy $r_B = \log_{10}(\tau_\nu/\tau_B)$, where τ_ν is the time of neutrino decoupling.

For priors on the magnetic quantities we choose a flat prior in $B_\lambda < 10$ nG. For r_B we use a flat prior with bounds $6 \leq r_B \leq 17$ corresponding to magnetic field production between the electroweak phase transition, and reheating at the GUT scale. Finally for the spectral index we use a flat prior $-2.95 \leq n_B \leq -1.6$, the lower bound of this comes from the fact that there is an infrared divergence for $n_B \leq -3$. The upper bound is from the fact that we are primarily interested in primordial fields produced in the early Universe (prior to nucleosynthesis), the work of [22] suggests that larger spectral indices are ruled out by nucleosynthesis constraints (see § IV D). Other than the upper bound on the spectral index, our results should be valid for fields produced at later epochs.

A. CMB only

Primordial magnetic fields contribute both passive and compensated scalar and tensor modes, as well as a compensated vector mode. However, the significant contributions are from the passive tensor mode, and the compensated vector mode, which are important on large and small scales respectively [8]. For comparison to CMB data (for scales $l \lesssim 3000$) we need only calculate these two.

We use the recent WMAP 7 year release [23] along with the final data from QUaD [24] and ACBAR [25] for $l < 3000$. We also use the Hubble Key Project data [26], BBN data, Union Supernova dataset [27] and BAO data from SDSS DR7 [28]. To account for the Sunyaev–Zel’dovich effect at high multipoles we adopt the standard treatment and use the WMAP template [23]. This requires an extra parameter for its normalisation A_{SZ} which we treat as a nuisance parameter and marginalise over.

The resulting constraints are shown in Fig. 4, which are in broad agreement with those of Ref. [12]. We have included only the magnetic amplitude B_λ and spectral index n_B , marginalising over the other parameters. The standard cosmological parameters are not shown as they are in agreement with their values in a universe with no primordial magnetic fields. We have also chosen not to include r_B as it is unconstrained by the data (see Fig. 5). This is a manifestation of the fact that the tensor passive mode can be only significant at large magnetic amplitudes, and these are already excluded by the magnetic vector mode. From this we calculate a 95% Confidence Limit of $B_\lambda < 6.4$ nG.

The constraints on the magnetic parameter space are unchanged when adding in large-scale matter power data sets such as 2dF [29] and SDSS LRG data from DR4 [30]³, though the cosmological parameters change as expected. The reason can be seen from Fig. 2, as the magnetic contributions are only significant for $k \gtrsim 1 h \text{Mpc}^{-1}$, and the galaxy redshift surveys probe only up to $k \sim 0.2 h \text{Mpc}^{-1}$. We will include this data for the remainder of this paper.

B. Sunyaev–Zel’dovich Effect

Recent work [19] has suggested that the Sunyaev–Zel’dovich (SZ) effect may be able to give tight constraints on the magnetic power spectrum. As the magnetic fields cause an increase in the small scale matter power spectrum, this gives rise to a large number of small mass halos and thus a rise in the SZ angular power spectrum. The recent release of data from the South Pole

² The modified version of CAMB and the adaptation of CosMoMC to use it will be available from <http://camb.info/jrs>.

³ We do not use the latest SDSS DR7 data [31] due to complications modifying its likelihood calculation to include the magnetic field matter power spectrum.

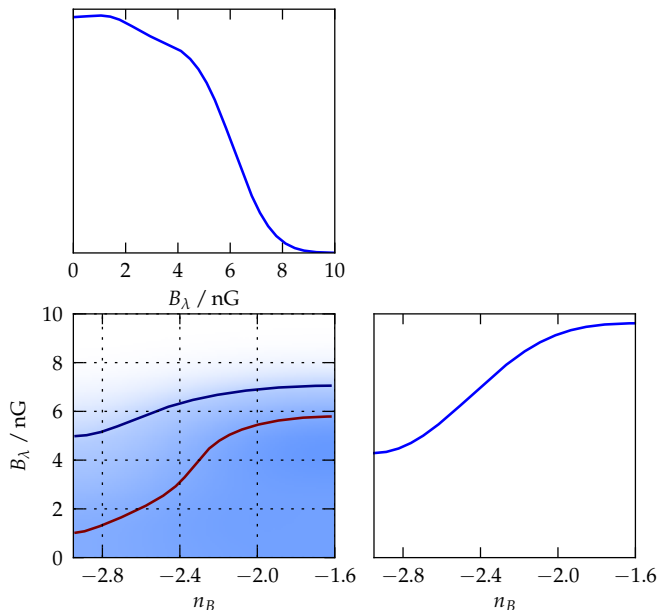


FIG. 4: The CMB only (WMAP7 + QUAD + ACBAR) constraints on the magnetic field amplitude and spectral index. The top left plot is the marginalised constraint solely on the magnetic field, and the bottom right is the marginal constraint on its spectral index. The bottom left plot is the joint constraint (marginalised over the other cosmological parameters), with contours for one and two sigma errors.

Telescope (SPT) [32], provides CMB observations up to $l \sim 10^4$ that we will compare to.

We follow the general method of [19], using the prescription of [33] to calculate the thermal SZ angular power spectrum from the matter power spectrum, which we have calculated using our modified version of CAMB. We give the details of this calculation in Appendix A. In addition to the SZ contribution the magnetic vector mode gives a significant addition to the small scale CMB power, which must be included. We do not include the kinetic SZ spectrum which is sub-dominant to the thermal spectrum. We also note that the non-gaussian statistics of the SZ effect can significantly increase its intrinsic variance [34]; we do not account for this within this paper.

As well as the datasets for the CMB-only constraints, and the SPT data, we have also included the large scale matter power data. When generating the SZ power spectrum we must include all contributions, both the adiabatic and magnetic contributions, as such we do not add in an SZ template, and thus A_{SZ} is no longer sampled over. The SPT data contains a further small scale contribution from the unresolved point sources, both from star-forming and radio galaxies (see Fig. 6). The exact value must be fit from the bandpowers (in the analysis of [32] it is poorly constrained with $C_l^{\text{ps}} = (6.2 \pm 6.4) \times 10^{-7} \mu\text{K}^2$). We expect that neglecting this contribution will have resulted in a small increase to our upper limits.

The magnetic contribution to the SZ power spectrum from our calculations is smaller than that of [19]. Dif-

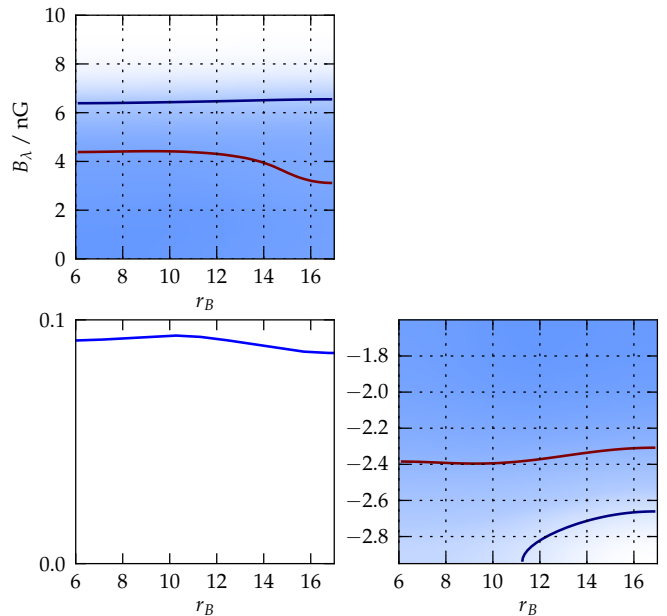


FIG. 5: The CMB-only marginal constraint on the production time ratio $r_B = \log_{10}(\tau_\nu/\tau_B)$ (bottom left), along with the correlations with the magnetic field amplitude (top left) and spectral index (bottom right). Even in the CMB-only constraint r_B is largely unconstrained and has minimal correlation with the other parameters, being only important in the case of very large magnetic fields, and a very red spectral index.

ferences between our calculations, such as in finding the amplitude of the matter perturbations and treating the non-linear effects, make it difficult to give a single reason for this.

Figure 7 shows the marginalised probability distributions for the magnetic parameters (again we do not plot r_B). The addition of the SPT data has excluded much of the parameter space that was allowed when including primary CMB effects only, especially the region with large magnetic field and blue spectral index, which gives the most dramatic change in the matter power spectrum (see Fig. 3). This gives a large decrease in the 95% CL of the magnetic amplitude to $B_\lambda < 4.1$ nG.

C. Lyman Alpha Data

It is clear from both Fig. 2 and Fig. 3 that the small scale matter power spectrum is significantly affected by the presence of a primordial magnetic field. Unfortunately galaxy redshift surveys such as SDSS probe only as far as $k \lesssim 0.2 h \text{ Mpc}^{-1}$, too large scales to be affected by the magnetic fields. However, observations of the Lyman- α flux power spectrum probe the matter density power spectrum to scales as small as $k \sim 5 h \text{ Mpc}^{-1}$, and may be able to give a much more powerful constraint. Unfortunately there is no simple analytic mapping from the observations to the matter spectrum, so cosmological

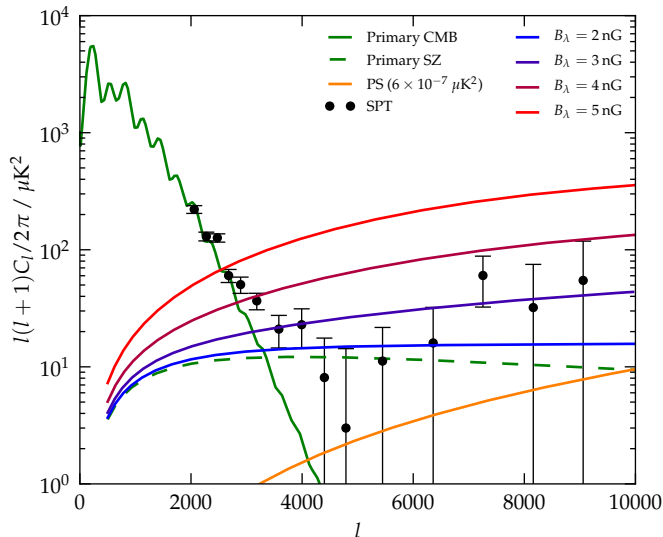


FIG. 6: The angular power spectrum of the CMB and the SZ contributions to it. We plot the SZ contribution from the primary adiabatic mode only, and in combination with four magnetic field strengths $B_\lambda = 2\text{--}5$ nG, with a magnetic spectral index of $n_B = -2.4$. We also plot the bandpowers from SPT, and the estimate of the residual point source contribution (labelled PS). Both the SZ contribution and the SPT data are at 150 GHz.

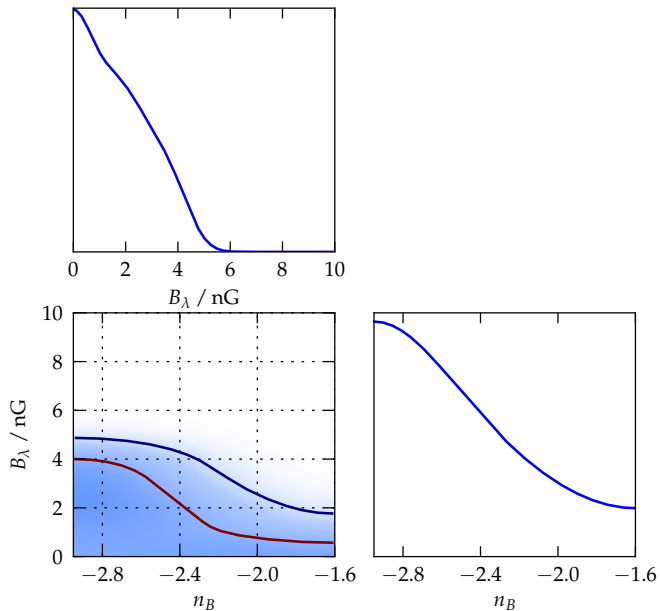


FIG. 7: The CMB and SZ constraints on the magnetic field amplitude and spectral index. The individual plots are equivalent to those in Fig. 4. Calculating the magnetic SZ contributions with the addition of SPT data has restricted the parameter space to lower amplitudes and redder spectral indices than the large scale CMB data.

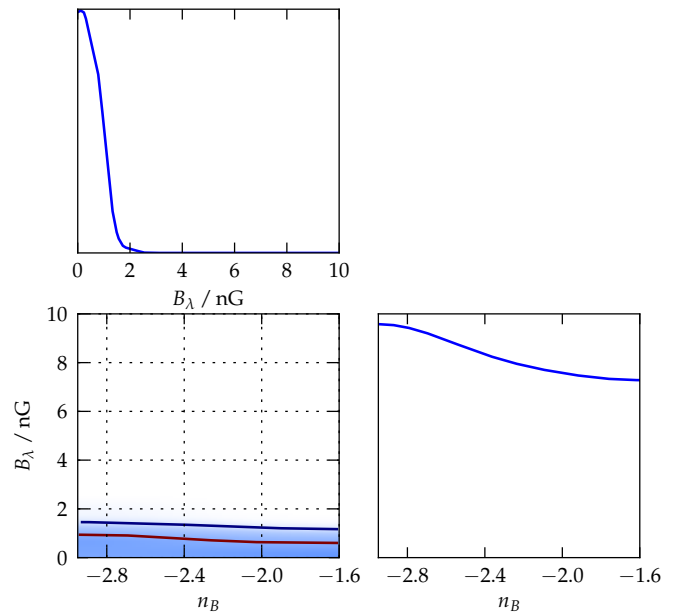


FIG. 8: Constraints on the magnetic field amplitude and spectral index using CMB and matter power data, including Lyman- α data. The Lyman- α data, which probes the small scale matter distribution, has dramatically reduced the allowable parameter space, to a range of small amplitudes ($B_\lambda \lesssim 1.5$ nG) roughly independent of spectral index n_B .

constraints need to be obtained by comparison to simulations [35]. A fully consistent analysis including magnetic fields is beyond the scope of this paper; instead we use a very rough simple approximation to the likelihood.

We use the standard Lyman- α module in COSMOMC which is based on the work of [35]. This finds an effective amplitude and spectral index about a pivot scale of $k = 0.009 \text{ s km}^{-1}$ (roughly $k \sim 1 h \text{ Mpc}^{-1}$). It calculates a likelihood from these by interpolating between a set of simulations compared to SDSS quasar data. Due to the large difference between our power spectra (when including magnetic effects) and those of Λ CDM we cannot expect the likelihoods to be very accurate, especially at large magnetic amplitudes and blue spectral indices, where the effect is greatest. However for the pivot scale, and range of scales probed by the SDSS spectra used $k \lesssim 0.02 \text{ s km}^{-1}$, the magnetic contribution is generally small compared to that of the primary adiabatic mode. In this light our results should be viewed as an approximation to the constraints that a more sophisticated likelihood approach would achieve.

The magnetic parameter space is significantly constrained by the use of the Lyman- α data (see Fig. 8), with the allowed region for B_λ being largely independent of the spectral index n_B . As the Lyman- α pivot scale ($k \sim 1 h \text{ Mpc}^{-1}$) coincides with the scale at which the magnetic matter power spectrum amplitudes are very similar across a large range of n_B this is to be expected. Overall this results in a 95% CL of $B_\lambda < 1.3$ nG.

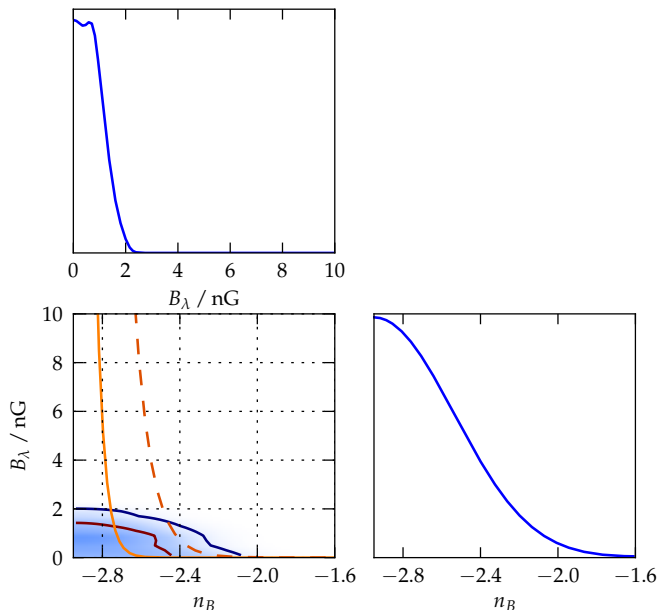


FIG. 9: Constraints on the magnetic parameter space from Lyman- α data including the nucleosynthesis constraints of [22]. The solid and dashed orange lines give the upper bounds in amplitude of a magnetic field produced at GUT scale inflation and the electroweak phase transition respectively. This corresponds to our priors.

D. Nucleosynthesis Constraints

Nucleosynthesis places strong constraints on the amount of energy density in gravitational waves allowed in the Universe, giving a limit of $\Omega_{\text{GW}} \lesssim 1.1 \times 10^{-6}$ [36]. As the anisotropic stress of an inhomogeneous magnetic field sources gravitational waves, this allows the small scale magnetic fields to transfer their energy into gravitational waves before being dissipated [22]. The limit on Ω_{GW} can therefore be used to constrain the magnetic field parameter space. We take Eq. (33) from [22] adapted to our conventions, yielding

$$B_\lambda / \text{nG} < 700 h \left[2^{\frac{n+5}{2}} \Gamma\left(\frac{n+5}{2}\right) \right]^{1/2} 10^{-\frac{n+3}{2}(4+r_B)}. \quad (29)$$

It is essential to note that this assumes that the magnetic field is well described by a single power law across a vast range of scales — from the pivot scale at $k = 1 \text{ Mpc}^{-1}$ up to at least $k = 10^{10} \text{ Mpc}^{-1}$, the horizon scale at the electroweak phase transition. Depending on how the magnetic field is generated this assumption may break down.

In Fig. 9 we show the probability distribution of the magnetic parameters when combining the nucleosynthesis constraint with the Lyman- α data of § IV C. As we would expect this reduces the allowed parameter spaces to redder spectral indices $n_B \lesssim -2$. Because of this the limits on the amplitude are slightly enlarged with the 95% CL becoming $B_\lambda < 1.6 \text{ nG}$.

V. CONCLUSION

As we have seen in this paper, when considering the magnetic contributions to the matter power spectrum it is essential to treat important small-scale, non-linear effects. We have demonstrated a technique for approximating the main non-linear effects within linear perturbation theory, and have incorporated this into a modified version of CAMB. This gives an alternative to the common approach of incorporating these effects directly into the initial power spectrum, such as in Ref. [12].

We have used our theoretical predictions to place constraints on the allowable magnetic field amplitude given various data sets. Where all limits are at 95% confidence, using CMB data only we find $B_\lambda < 6.4 \text{ nG}$, with a redder spectral index favoured. As the presence of a stochastic magnetic field gives significant modifications to the small scale matter distribution, we also look at the constraints when adding two probes of it: the Sunyaev–Zel’dovich effect measured by SPT [32], which gives a limit of $B_\lambda < 4.1 \text{ nG}$; and Lyman- α forest data from SDSS [35], which gives a rough constraint of $B_\lambda \lesssim 1.3 \text{ nG}$.

Whilst the addition of the small-scale matter data gives a large reduction in the allowed amplitude of a primordial magnetic field (certainly when using Lyman- α data), this is still roughly consistent with a scenario where current galactic fields are formed solely by adiabatic contraction of primordial fields. Increasing the accuracy of measurements at the scales we can currently probe with data will provide limited gains: since the magnetic power spectrum increases with B_λ^4 , significantly decreasing the errors on matter power spectrum measurements will produce less impressive gains in the upper limit on B_λ . However, if better observations and modelling allow accurate comparison to smaller scales there should be an almost linear decrease in the upper limit with the smallest scale probed. This would seem to provide the best opportunity for testing the primordial field hypothesis.

Our modifications to CAMB to for calculating the magnetic matter CMB and matter power spectra, as well as the general halo mass function and SZ power spectrum will shortly be available from <http://camb.info/jrs>. The modifications to integrate them into COSMOMC will be placed at the same location.

Acknowledgements

We would like to thank Steven Gratton, Simeon Bird, Chiara Caprini and Camille Bonvin for useful discussion. JRS is supported by an STFC studentship. AL acknowledges a PPARC/STFC advanced fellowship.

Appendix A: Sunyaev—Zel’dovich Effect

In order to compare to the recent data from the South Pole Telescope [32], we need to be able to calculate SZ

angular power spectra from linear matter power spectra. We use the halo method of Komatsu and Seljak [33], and largely follow details of the calculation in [32]. We give an outline of this below.

The angular power spectrum is given by

$$C_l = g_\nu^2 \int dz \frac{dV_c}{dz} \int dM \frac{dn(M, z)}{dM} |y_l(M, z)|^2. \quad (\text{A1})$$

In the above V_c is the comoving volume out to redshift z , and g_ν is the spectral function given by

$$g_\nu = \frac{x}{\tanh(x/2)} - 4 \quad (\text{A2})$$

where $x = h\nu/k_B T_{\text{CMB}}$. The halo mass function $\frac{dn}{dM}$ is comoving number density of virialized halos at mass M . Finally y_l is the Fourier transform of the projected Compton y profile

$$y_l(M, z) = \frac{4\pi r_s}{l_s^2} \int_0^\infty y_{3D}(x) \text{sinc}(lx/l_s) x^2 dx, \quad (\text{A3})$$

where r_s is the scale radius of the profile, $l_s = d_a/r_s$ is its angular projection (d_a is the angular diameter distance to redshift z) and y_{3D} is the three-dimensional Compton profile in terms of $x = r/r_s$. The profile y_{3D} is determined by the model chosen for the baryon density and temperature profile of the halo. To find it we follow the details of [33], fixing its form with four assumptions: the dark matter density profile is NFW [37]; hydrostatic equilibrium between the gas pressure and the halo self-gravity; baryon density traces the dark matter density in the outer halo; and the gas has a polytropic equation of state $P_b \propto \rho_b^\gamma$. The results of this are given below, for details see [33].

Using an NFW dark matter profile, the scale radius above r_s is the usual NFW definition, $r_s = r_{\text{vir}}/c$ where c is the concentration, and r_{vir} is the virial radius given by

$$r_{\text{vir}} = \left(\frac{3}{4\pi} \frac{M}{\Delta_c \rho_{\text{cr}}} \right)^{1/3}, \quad (\text{A4})$$

where the virialisation parameter Δ_c can be calculated from the spherical collapse of a top hat perturbation. A fitting formula for Δ_c is calculated in [38]

$$\Delta_c(z) = 18\pi^2 - 82\Omega_\Lambda(z) + 39\Omega_\Lambda(z)^2 \quad (\text{A5})$$

which is accurate in the range $\Omega_\Lambda < 0.9$.

The concentration parameter c which defines the scale radius of the profile can be fitted from simulations. We use the relation of [39] which takes the form

$$c(M, z) \approx \frac{7.85}{(1+z)^{0.71}} \left(\frac{M}{M_*} \right)^{-0.081}, \quad (\text{A6})$$

where the pivot mass is fixed to be $M_* = 2 \times 10^{12} h^{-1} M_\odot$.

The profile y_{3D} is given by

$$y_{3D}(x) = 1.14 \times 10^{-4} \text{Mpc}^{-1} \times \left[\frac{\rho_b(0)}{10^{14} M_\odot \text{Mpc}^{-3}} \right] \left[\frac{k_B T_b(0)}{8 \text{keV}} \right] y(x). \quad (\text{A7})$$

The dimensionless function $y(x)$ gives the profile shape

$$y(x) = \left[1 - B[1 - x^{-1} \ln(1+x)] \right]^{\gamma/(\gamma-1)}. \quad (\text{A8})$$

B is a constant given by

$$B \equiv 3\eta^{-1} \frac{\gamma-1}{\gamma} \left[\frac{1}{c} \ln(1+c) - \frac{1}{1+c} \right]^{-1} \quad (\text{A9})$$

Fitting functions for η and γ are derived in [33]. They are valid for the range $1 < c < 25$:

$$\gamma = 1.137 + 0.0894 \ln(c/5) - 3.68 \times 10^{-3}(c-5), \quad (\text{A10})$$

$$\eta = 2.235 + 0.202(c-5) - 1.16 \times 10^{-3}(c-5)^2. \quad (\text{A11})$$

The central gas density $\rho_b(0)$ is

$$\rho_b(0) = 7.96 \times 10^{12} M_\odot \text{Mpc}^{-3} \left(\frac{M}{10^{14} M_\odot} \right) \left(\frac{r_{\text{vir}}}{\text{Mpc}} \right)^3 \times \left(\frac{\Omega_b}{\Omega_m} \right) \frac{y(x)^{-1/\gamma}}{(1+c)^2} \left[\frac{1}{c} \ln(1+c) - \frac{1}{1+c} \right]^{-1}, \quad (\text{A12})$$

and the central temperature $T_b(0)$ is

$$T_b(0) = 0.880 \text{keV} \eta \left(\frac{M}{10^{14} M_\odot} \right) \left(\frac{r_{\text{vir}}}{\text{Mpc}} \right)^{-1}. \quad (\text{A13})$$

The final ingredient needed to calculate the SZ power spectrum is the mass function. In common with [32, 33] we use the Jenkins mass function [40] calculated from N-body simulations. As with the Press-Schechter prescription the key quantity is the smoothed variance $\sigma(R)$ defined by

$$\sigma^2(R; z) = \int d \ln k \widetilde{W}_R^2(k) \mathcal{P}(k; z). \quad (\text{A14})$$

In our work we choose a window function $\widetilde{W}_R(k)$ that is a spherical top hat in real space. The mass enclosed in this comoving scale is simply $M = 4\pi \rho_{m,0} R^3/3$, and this defines an obvious mapping between a mass smoothed $\sigma(M)$ and $\sigma(R)$. In terms of $\sigma(M)$ the mass function of [40] is

$$\frac{M^2}{\rho_{m,0}} \frac{dn(M; z)}{dM} = 0.301 \left| \frac{d \ln \sigma}{d \ln M} \right| \exp \left(-|0.64 - \ln \sigma| \right) \quad (\text{A15})$$

-
- [1] L. M. Widrow, *Reviews of Modern Physics* **74**, 775 (2002), arXiv:astro-ph/0207240.
 - [2] R. M. Kulsrud and E. G. Zweibel, *Reports on Progress in Physics* **71**, 046901 (2008), 0707.2783.
 - [3] M. L. Bernet, F. Miniati, S. J. Lilly, P. P. Kronberg, and M. Dessauges-Zavadsky, *Nature* **454**, 302 (2008), 0807.3347.
 - [4] K. Subramanian and J. D. Barrow, *Phys. Rev. Lett.* **81**, 3575 (1998), arXiv:astro-ph/9803261.
 - [5] F. Finelli, F. Paci, and D. Paoletti, *Phys. Rev. D* **78**, 023510 (2008), 0803.1246.
 - [6] D. Paoletti, F. Finelli, and F. Paci, *ArXiv e-prints* (2008), 0811.0230.
 - [7] D. G. Yamazaki, K. Ichiki, T. Kajino, and G. J. Mathews, *Phys. Rev. D* **77**, 043005 (2008), 0801.2572.
 - [8] J. R. Shaw and A. Lewis, *Phys. Rev. D* **81**, 043517 (2010), 0911.2714.
 - [9] D. G. Yamazaki, K. Ichiki, K. Umezu, and H. Hanayama, *Phys. Rev. D* **74**, 123518 (2006), arXiv:astro-ph/0611910.
 - [10] D. G. Yamazaki, K. Ichiki, T. Kajino, and G. J. Mathews, *ApJ* **646**, 719 (2006), arXiv:astro-ph/0602224.
 - [11] D. G. Yamazaki, K. Ichiki, T. Kajino, and G. J. Mathews, *Phys. Rev. D* **81**, 023008 (2010), 1001.2012.
 - [12] D. Paoletti and F. Finelli, *ArXiv e-prints* (2010), 1005.0148.
 - [13] R. Durrer, *Fundamentals of Cosmic Physics* **15**, 209 (1994), arXiv:astro-ph/9311041.
 - [14] R. Durrer and N. Straumann, *Helv. Phys. Acta* **61**, 1027 (1988), arXiv:astro-ph/9311041.
 - [15] K. Subramanian and J. D. Barrow, *Phys. Rev. D* **58**, 083502 (1998), arXiv:astro-ph/9712083.
 - [16] K. Jedamzik, V. Katalinić, and A. V. Olinto, *Phys. Rev. D* **57**, 3264 (1998), arXiv:astro-ph/9606080.
 - [17] E. Kim, A. V. Olinto, and R. Rosner, *ApJ* **468**, 28 (1996), arXiv:astro-ph/9412070.
 - [18] J. D. Barrow, R. Maartens, and C. G. Tsagas, *Phys. Rep.* **449**, 131 (2007), arXiv:astro-ph/0611537.
 - [19] H. Tashiro and N. Sugiyama, *ArXiv e-prints* (2009), 0908.0113.
 - [20] A. Lewis, A. Challinor, and A. Lasenby, *ApJ* **538**, 473 (2000), arXiv:astro-ph/9911177.
 - [21] A. Lewis and S. Bridle, *Phys. Rev. D* **66**, 103511 (2002), astro-ph/0205436.
 - [22] C. Caprini and R. Durrer, *Phys. Rev. D* **65**, 023517 (2002), arXiv:astro-ph/0106244.
 - [23] N. Jarosik, C. L. Bennett, J. Dunkley, B. Gold, M. R. Greason, M. Halpern, R. S. Hill, G. Hinshaw, A. Kogut, E. Komatsu, et al., *ArXiv e-prints* (2010), 1001.4744.
 - [24] M. L. Brown, P. Ade, J. Bock, M. Bowden, G. Cahill, P. G. Castro, S. Church, T. Culverhouse, R. B. Friedman, K. Ganga, et al., *ApJ* **705**, 978 (2009), 0906.1003.
 - [25] C. L. Reichardt, P. A. R. Ade, J. J. Bock, J. R. Bond, J. A. Brevik, C. R. Contaldi, M. D. Daub, J. T. Dempsey, J. H. Goldstein, W. L. Holzapfel, et al., *ApJ* **694**, 1200 (2009), 0801.1491.
 - [26] W. L. Freedman et al., *Astrophys. J.* **553**, 47 (2001), astro-ph/0012376.
 - [27] M. Kowalski et al. (2008), 0804.4142.
 - [28] W. J. Percival et al. (2009), 0907.1660.
 - [29] S. Cole et al. (The 2dFGRS), *Mon. Not. Roy. Astron. Soc.* **362**, 505 (2005), astro-ph/0501174.
 - [30] M. Tegmark et al., *Phys. Rev. D* **74**, 123507 (2006), astro-ph/0608632.
 - [31] B. A. Reid et al. (2009), 0907.1659.
 - [32] M. Lueker, C. L. Reichardt, K. K. Schaffer, O. Zahn, P. A. R. Ade, K. A. Aird, B. A. Benson, L. E. Bleem, J. E. Carlstrom, C. L. Chang, et al., *ArXiv e-prints* (2009), 0912.4317.
 - [33] E. Komatsu and U. Seljak, *MNRAS* **336**, 1256 (2002), arXiv:astro-ph/0205468.
 - [34] P. Zhang and R. K. Sheth, *Astrophys. J.* **671**, 14 (2007), astro-ph/0701879.
 - [35] P. McDonald, U. Seljak, R. Cen, D. Shih, D. H. Weinberg, S. Burles, D. P. Schneider, D. J. Schlegel, N. A. Bahcall, J. W. Briggs, et al., *ApJ* **635**, 761 (2005), arXiv:astro-ph/0407377.
 - [36] M. Maggiore, *ArXiv General Relativity and Quantum Cosmology e-prints* (2000), arXiv:gr-qc/0008027.
 - [37] J. F. Navarro, C. S. Frenk, and S. D. M. White, *Astrophys. J.* **490**, 493 (1997), astro-ph/9611107.
 - [38] G. L. Bryan and M. L. Norman, *ApJ* **495**, 80 (1998), arXiv:astro-ph/9710107.
 - [39] A. R. Duffy, J. Schaye, S. T. Kay, and C. Dalla Vecchia, *MNRAS* **390**, L64 (2008), 0804.2486.
 - [40] A. Jenkins, C. S. Frenk, S. D. M. White, J. M. Colberg, S. Cole, A. E. Evrard, H. M. P. Couchman, and N. Yoshida, *MNRAS* **321**, 372 (2001), arXiv:astro-ph/0005260.